The Impacts of Source Location in Tomographic Gamma Scanning – 17324

J. M. Kirkpatrick*, D. Nakazawa*, S. K. Smith**, L. Tondut***, P. McClay*,
D. Petroka*, M. Villani*, X. Ducoux*, S. Philips*

*Mirion Technologies - Canberra Industries, Inc.
**Oak Ridge National Laboratory
***AREVA NC La Hague

ABSTRACT

Canberra Industries has recently designed and built a Tomographic Gamma Scanning (TGS) system for the deployment in a nuclear facility. The TGS technique combines high-resolution gamma spectroscopy with low spatial resolution 3-dimensional image reconstruction to provide increased accuracy over traditional approaches for the assay of non-uniform source distributions in low-to medium-density containers. The TGS system has been optimized to measure 120 liter drums and has been equipped to use various collimators and attenuators to assay containers under a wide range of operational conditions.

In this paper, we report on experimental work using TGS systems aimed at evaluating the effects of source locations at the limits of volume elements, or voxels, defined in the image reconstruction. These include sources placed at voxel boundaries within a single vertical layer and sources placed in the lowest and highest possible vertical positions within the containers. Building upon previous studies, the accuracy of the TGS system was also assessed by varying the radial position of a point source within a vertical segment. The robustness of the TGS image reconstruction algorithm to location of the sources location was also analyzed as a function of matrix density and gamma-ray energy. Methods to reduce the biases from source location at extreme positions within the container were implemented and tested. The results from this work have been used to better understand the total measurement uncertainty (TMU) and analysis methodology used in TGS systems currently deployed and under development.

INTRODUCTION

Industrial TGS systems have been commercially employed for the characterization of radioactive waste generated by facilities handling special nuclear materials (SNM) and nuclear power plants [1-3]. A recent system was constructed and commissioned to assay 120 liter drums for a nuclear facility using a variety of collimator openings and spatial reconstruction mappings [4-5]. A key feature of any TGS system is its ability to localize gamma-emitting material within the container and provide proper attenuation corrections from surrounding material, both on a volume element (voxel) basis. Previous studies have explored the limits of accuracy of this localization and quantification for 200 liter drums and smaller containers [6-7]. This paper extends both the analysis and measurements using the most recent system to investigate the impact of the size of the container, the collimation aperture, and the defined voxel size in the image reconstruction.

TGS data acquisition consists of a synchronized scanning of the cylindrical container with radioactive waste in three degrees of freedom: vertical, rotation, and translation. The item is continuously rotated and translated across the field of view of a collimated High Purity Germanium (HPGe) detector and a transmission source while a large number of full spectral grabs or view data are acquired. This scanning is done both with a transmission source shining from opposite side of the detector through the item and with the source blocked. These two scans, transmission and emission, respectively, contain the necessary information to perform image reconstruction of both the gamma emitters and their attenuated rays through the drum contents. This analysis is performed on for predefined gamma energies of interest in both the calibration of the system response with known sources and sources of interest in unknown assay items.

Following the calibration process of the system, a wide range of assays were performed with point sources placed at various radii and vertical heights within different matrices to investigate the system response as a function of source location. Quantification of the impacts of source location on the total measurement uncertainty is presented for this TGS system. This paper concludes with a discussion comparing results of other systems, highlighting new developments from the current study, and the direction of on-going work.

SYSTEM HARDWARE AND SOFTWARE

The TGS system used in this study is comprised of 3 main assemblies: the transmission source vertical lift, the rotator-translator table, and the detector vertical lift with electrical cabinet. The vertical lifts for the transmission source and detector assembly are synchronized for each TGS assay. A schematic of the full system is shown in the figure below (Fig. 1).

The TGS collimator inserts, 25.4 mm (1”) and 12.7 mm (0.5”) must be replaced manually to switch between the standard TGS spatial resolution (10x10 voxels per vertical layer) and the higher resolutions (14x14 & 20x20), respectively. A switch on the back of the attenuator assembly must be accordingly set as this is the only way for the Programmable Logic Controller (PLC) and NDA 2000 software to register the collimator positioned within the system. This is critical for the data acquisition and image reconstruction algorithms.

The detector distance with respect to the drum is changed by a manual ball screw, which moves the entire detector/attenuator/collimator assembly. The total length of travel available is 355.6 mm (14”). The operator is guided in the detector positioning by a ruler and labels next to the detector position drive crank.

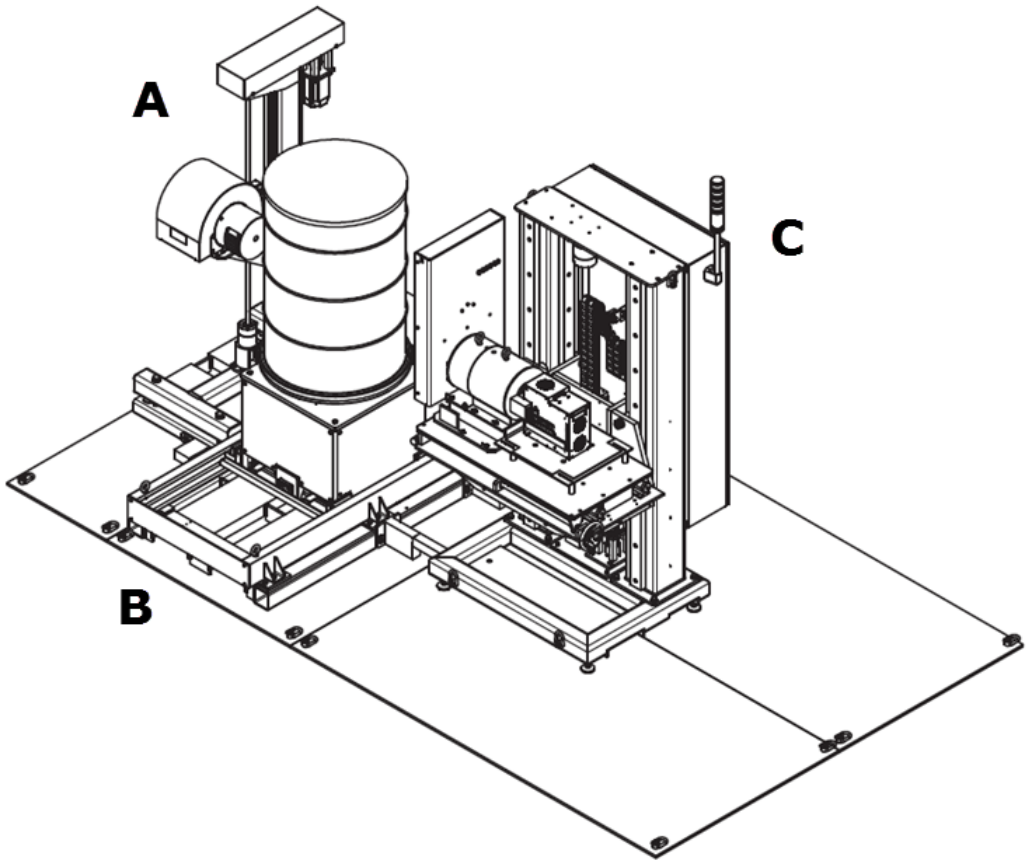

Figure 1. A schematic of the TGS system. The assembly (A) on the left houses the transmission source. The center assembly (B) is the rotator-translator with a drum positioned atop, and the right assembly (C) is the detector lift with collimator and attenuators.

The last component of the geometry is the attenuator assembly. Three attenuators are available for use in order to reduce emission count rates from highly active assay items. Typically, a system with attenuators has only 4 attenuator positions: Open, attenuator 1 down, attenuators 1 & 2 down, and all attenuators down. Any combination of the three attenuators can be down or up, yielding eight possible combinations. More details of all three assemblies can be found in [4].

TGS Calibration

The TGS system was calibrated for the 120 L container with three spatial resolutions: 10x10x30, 14x14x20, and 20x20x21. Further details on the TGS calibration methodology and analysis can be found in [4-5]. The 120 L container has a height of 73 cm and an inner diameter of 46 cm. Assays to study the effects of point source location within the container for this paper were taken with the 10x10x30 resolution geometry. By defining the spatial resolution as 10x10x30 volume elements, the dimensions of each reconstructed element are 4.9 cm in length and width and 2.5 cm in height.

The figure below shows the distribution of the calibration assay errors about the mean value of the response for the 10x10x30 geometry with various drums (Figure

2). FM stands for a foam matrix drum with a bulk density of 0.03 g/cc. SB stands for softboard material, which has a density of 0.39 g/cc. MDF stands for medium-density fiber board, having a density of 0.68 g/cc. For the calibration effort, both rod and point sources containing Ba-133, Cs-137, and Co-60 were used.

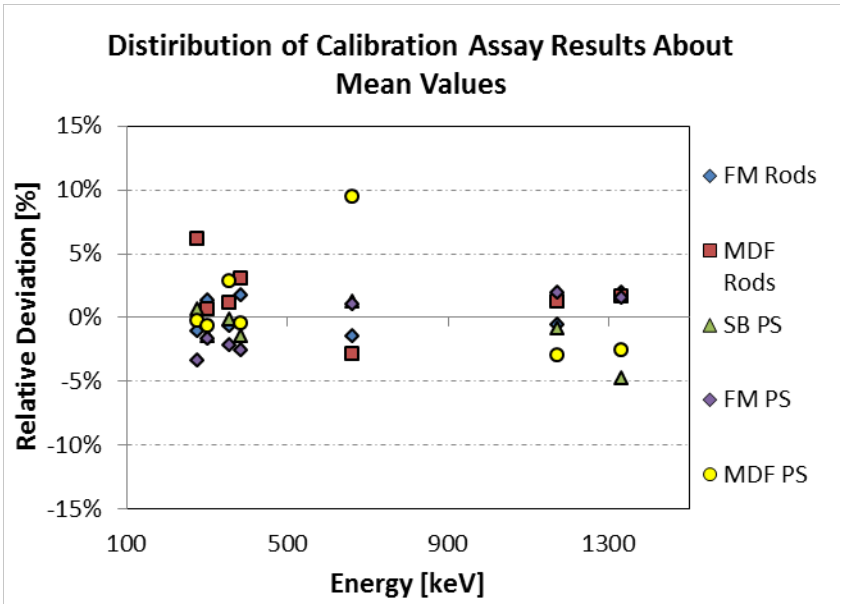

Figure 2. Calibration Assay Deviation with respect to the mean as a function of energy and drum material.

EXPERIMENTAL SETUP

For the source location study, the point sources were placed in various locations within the three matrix types (foam, softboard, and fiberboard) to study the effects of radial position and extreme locations. Each of the point sources are contained in a stainless less capsule (A3011 type), measuring 3.65 cm long with an outer diameter of 0.95 cm. A total of three Ba-133 sources were used, each containing approximately 3.4 MBq of activity. A single Cs-137 source (1.96 MBq) and a single Co-60 source were also employed (1.84 MBq).

The drum was divided into three evenly spaced vertical sections: top, middle, and bottom. The matrices also contained holes drilled at various radii to vary the location along the radial axis. The following tables describe the radial location definitions (Table 1) and the each of the assays performed in each matrix by the location of the sources (Table 2).

Table 1. Definition of radial position within the 120 L drums, corresponding to various holes drilled into each of the matrices.

Radial Position	Distance from Center (cm)	Vertical Position	Height from Bottom (cm)
R1	0.0	V1	0.0
R2	6.6	V2	12.0
R3	11.5	V3	24.0
R4	14.9	V4	36.0
R5	17.6	V5	48.0
R6	19.9	V6	60.0
R7	20.6	V7	72.0
R8	20.9		
R9	21.4		

Table 2. Position of point sources for each assay conducted in this study. FM, SB, and MDF stand for the foam matrix, softboard, and fiberboard, respectively. The radial and vertical positions corresponds to those in Table 1.

Assay Number	Matrix Type	Ba-133 #1	Ba-133 #2	Ba-133 #3	Cs-137	Co-60
1	FM	R3, V2	R8, V4	R8, V6	R9, V5	R8, V2
2	FM	R1, V4	R2, V4	R3, V4	R9, V1	R8, V7
3	FM	R2, V4	R4, V4	R5, V4	R3, V2	R9, V6
4	FM	R3, V5	R5, V5	R7, V3	R6, V4	R4, V5
5-8	SB	R2, V6	R4, V2	R8, V4	R5, V4	R6, V2
9-11	SB	R3, V5	R5, V3	R7, V5	R6, V4	R4, V5
12	SB	R4, V2	R4, V4	R4, V6	R6, V2	R2, V1
13	SB	R4, V2	R4, V4	R4, V6	R6, V2	R2, V1
14	MDF	R8, V2	R9, V4	R3, V6	R8, V4	R9, V2
15	MDF	R2, V4	R4, V4	R5, V4	R8, V2	R8, V1
16-18	MDF	R1, V4	R2, V4	R4, V4	R9, V7	R8, V1
19	MDF	R2, V4	R4, V4	R5, V4	R3, V7	R8, V2
20	MDF	R2, V1	R4, V1	R5, V1	R3, V6	R8, V2
21-22	MDF	R2, V4	R4, V4	R5, V4	R6, V2	R2, V2

It should be noted that many of the assays are replicates in terms of radial position and height of the sources. In these cases, the starting angular orientation of the drum on the rotator with respect to the detector and transmission axis was varied and the point sources were removed and placed back into position for each assay.

RESULTS AND ANALYSIS

The analysis of the measurements is divided into three broad categories to evaluate the performance of the TGS system with respect to source position in a variety of drum materials.

First, the uncertainty of source location is separated from matrix type by grouping together the measurements for each matrix and calculating the variance in responses with respect to the mean and the expected response from the sources. Next, matrix effects are quantified by comparing the full reconstructed response in a given layer for the homogenous matrix materials to a constant attenuation correction factor. Finally, an uncertainty for slight deviations in the TGS image reconstruction is estimated to account for activity placed in an adjacent voxel to where the source is physically located. These are then combined for a total measurement uncertainty (TMU) for the system and compared to similar analyses performed on previous systems.

Source Location Uncertainty

Source location error is a broad term that covers the error produced by the TGS technique for point sources located within a container. This is equivalent to the source non-uniformity uncertainty term for other NDA systems. After calculation of the relative uncertainty among the wide range of assays and source locations, this uncertainty is intended to be combined with other components, such as matrix effects and calibration errors, to determine the total measurement uncertainty of the system.

First, the measurement results are selected in two broad categories: those with locations at extreme vertical positions defined as either V1 or V7 in Table 1 and those located between V2 and V6. The purpose of this is primarily to be able to compare to the previous study of the source location error with a 200 L drum TGS system [6]. In that paper, no sources were placed at the upper and lower extremes of the container.

The values for each of the gamma energy regions of interest shown in Tables 3 through 5 represent the calibrated response from the TGS system in units of TGS number. This TGS number is the sum of the reconstructed, attenuation count rates at each energy region of interest (ROI) for all the voxels within the drum. Using the calibration shown in Figure 2, an expected response is also displayed in the tables. The relative uncertainty is calculated as the standard deviation of the measurements divided by the average response. If only a single point is used, a factor of $1/\sqrt{3}$ can be applied to this component in the uncertainty analysis, following a generally accepted assumption that waste items do not contain isolated, single sources [6].

As the sample size for the calculation of the relative uncertainty is small, and likely does not represent a normal distribution, a one-sided chi-square test was performed to verify if the variability of our sample is no greater than the variability of the uncertainty term calculated in [6], with the $1/\sqrt{3}$ factor.

Table 3. Source Location Response and Uncertainty for Foam Drum Excluding Top and Bottom Layers.

Assay Number	276 keV	303 keV	356 keV	384 keV	662 keV	1173 keV	1333 keV
1	0.365	0.861	2.647	0.385	0.494	0.409	0.388
2	0.305	0.711	2.136	0.323	N/A	N/A	N/A
3	0.343	0.807	2.415	0.345	0.469	0.41	0.407
4	0.336	0.812	2.466	0.361	0.461	0.409	0.418
Average	0.337	0.798	2.416	0.354	0.475	0.409	0.404
Expected Response	0.327	0.787	2.400	0.330	0.476	0.410	0.394
Standard Deviation	0.0248	0.0628	0.2116	0.0261	0.0099	0.0003	0.0088
$1/\sqrt{3}$	No	No	No	No	Yes	Yes	Yes
Relative Uncertainty	7.4%	7.9%	8.8%	7.4%	2.1%	0.1%	2.2%

Table 4. Source Location Response and Uncertainty for Softboard Drum Excluding End Effects.

Assay Number	276 keV	303 keV	356 keV	384 keV	662 keV	1173 keV	1333 keV
5	0.33	0.79	2.444	0.337	0.456	0.418	0.394
6	0.348	0.819	2.448	0.352	0.465	0.401	0.389
7	0.346	0.799	2.508	0.336	0.458	0.394	0.401
8	0.359	0.844	2.515	0.348	0.464	0.399	0.405
9	0.361	0.825	2.497	0.359	0.47	0.387	0.400
10	0.33	0.825	2.475	0.351	0.493	0.396	0.400
11	0.339	0.823	2.449	0.337	0.494	0.407	0.390
12	0.339	0.756	2.265	0.321	0.475	N/A	N/A
13	0.343	0.842	2.532	0.343	0.482	N/A	N/A
Average	0.344	0.814	2.459	0.343	0.473	0.400	0.397
Expected Response	0.327	0.787	2.400	0.330	0.476	0.410	0.394
Standard Deviation	0.0111	0.0278	0.0796	0.0113	0.0081	0.0058	0.0035
$1/\sqrt{3}$	No	No	No	No	Yes	Yes	Yes
Relative Uncertainty	3.2%	3.4%	3.2%	3.3%	1.7%	1.4%	0.9%

Table 5. Source Location Response and Uncertainty for Medium Density Fiberboard Drum Excluding End Effects.

Assay Number	276 keV	303 keV	356 keV	384 keV	662 keV	1173 keV	1333 keV
14	0.327	0.797	2.517	0.340	0.493	0.409	0.403
15	0.292	0.68	2.278	0.303	0.521	N/A	N/A
16	0.254	0.622	2.068	0.272	N/A	N/A	N/A
17	0.274	0.635	2.246	0.269	N/A	N/A	N/A
18	0.270	0.663	2.131	0.294	N/A	N/A	N/A
19	0.312	0.794	2.415	0.339	N/A	0.403	0.39
20	N/A	N/A	N/A	N/A	0.436	0.399	0.355
21	0.315	0.781	2.58	0.346	0.442	0.357	0.363
22	0.323	0.788	2.4	0.333	0.502	0.449	0.421
Average	0.296	0.720	2.329	0.312	0.479	0.403	0.386
Standard Deviation	0.0274	0.0769	0.1803	0.0315	0.0218	0.0189	0.0159
Expected Response	0.327	0.787	2.400	0.330	0.476	0.410	0.394
$1/\sqrt{3}$	No	No	No	No	Yes	Yes	Yes
Relative Uncertainty	9.3%	10.7%	7.7%	10.1%	4.6%	4.7%	4.1%

The test statistic, T, is calculated as:

$$T = (N-1) * \left(\frac{s}{\sigma_o}\right)^2 \quad (1)$$

where *N* is the sample size, *s* is the sample relative standard deviation, and σ_0 is the target relative standard deviation corrected for 3 point sources. For the target uncertainty, the empty drum uncertainty component from [6] was used (first row in Table 6). The test statistic is compared to the critical value of the chi-square distribution with N-1 degrees of freedom.

$$T > \chi^2_{\alpha,N-1} \quad (2)$$

where *α* is the significance level. The significance level chosen for the comparison is 95%. When height extremes were not included, the majority of the nuclide ROI energies over all 3 densities passed the test. Table 6 shows the results of the statistical tests for the three matrix types.

Table 6. Chi-Square Test of Source Location Error .

	276 keV	**303 keV**	**356 keV**	**384 keV**	**662 keV**	**1173 keV**	**1333 keV**
Target Drum Unc. (%)	7%	13%	11%	10%	6%	8%	8%
FM T Value	9.485	3.151	5.417	5.264	0.782	0.001	0.391
FM X^2	7.815	7.815	7.815	7.815	5.991	5.991	5.991
FM T Test	Fails	True	True	True	True	True	True
SB T Value	4.831	1.588	1.972	2.814	2.119	0.560	0.194
SB X^2	15.507	15.507	15.507	15.507	15.507	12.592	12.592
SB T Test	True	True	True	True	True	True	True
MDF T Value	35.052	13.564	9.878	22.946	7.403	3.969	2.809
MDF X^2	14.067	14.067	14.067	14.067	9.488	9.488	9.488
MDF T Test	Fails	True	True	Fails	True	True	True

When the extreme height positions are included in the source location error analysis, the uncertainty values and test statistics change by a significant amount. Again, for the Cs-137 and Co-60 ROIs, the standard deviation was divided by square root of three based on the 3 point sources postulate. Tables 7 through 9 display the relevant relative for the three matrix types, along with the associated statistical T test results as well.

Table 7. Source Location Uncertainty for Foam Drum With End Effects for the Cs-137 and Co-60 sources. The Ba-133 sources were not placed in the bottom or top of the foam drum.

Assay Number	**662 keV**	**1173 keV**	**1333 keV**
1	0.494	0.409	0.388
2	0.411	0.299	0.298
3	0.469	0.41	0.407
4	0.461	0.409	0.418
Average	0.459	0.382	0.378
Standard Deviation	0.0201	0.0319	0.0315
Relative Uncertainty	4.4%	8.3%	8.3%
T Value	5.133	9.448	8.705
X^2	7.815	7.815	7.815
T test Result	True	Fails	Fails

Table 8. Source Location Uncertainty for Softboard Drum with End Effects for the Co-60 source. The Ba-133 and Cs-137 sources were not placed in the bottom or top of the foam drum.

Assay Number	1173 keV	1333 keV
5	0.418	0.394
6	0.401	0.389
7	0.394	0.401
8	0.399	0.405
9	0.387	0.4
10	0.396	0.4
11	0.407	0.39
12	0.279	0.265
13	0.272	0.276
Average	0.373	0.369
Standard Deviation	0.0322	0.0324
Relative Uncertainty	8.6%	8.8%
T Value	26.989	25.700
X^2	15.507	15.507
T test Result	Fails	Fails

Table 9. Source Location Response and Uncertainty for Medium Density Fiberboard Drum with End Effects.

Assay Number	276 keV	303 keV	356 keV	384 keV	662 keV	1173 keV	1333 keV
14	0.327	0.797	2.517	0.34	0.493	0.409	0.403
15	0.292	0.68	2.278	0.303	0.521	0.403	0.383
16	0.254	0.622	2.068	0.272	0.534	0.395	0.386
17	0.274	0.635	2.246	0.269	0.568	0.349	0.348
18	0.27	0.663	2.131	0.294	0.528	0.36	0.378
19	0.312	0.794	2.415	0.339	0.451	0.403	0.39
20	0.194	0.731	2.398	0.274	0.436	0.399	0.355
21	0.333	0.765	2.518	0.346	0.521	0.259	0.27
22	0.315	0.781	2.58	0.346	0.442	0.357	0.363
Average	0.286	0.719	2.350	0.309	0.499	0.370	0.364
Standard Deviation	0.0438	0.0698	0.1799	0.0336	0.0269	0.0275	0.0227
Relative Uncertainty	15%	10%	8%	11%	5%	7%	6%
T Value	109.863	12.795	11.045	30.369	20.696	19.992	13.014
X^2	15.507	15.507	15.507	15.507	15.507	15.507	15.507
T test Result	Fails	True	True	Fails	Fails	Fails	True

It should be noted that the largest deviations from the expected response from the point sources arises from sources resting on the bottom of the drum. It is not surprising that when the statistical T test is calculated using the expected measurement uncertainty derived from a previous system that did not include any measurements with sources at the very bottom of the container, more of the T test comparisons fail. Performing more extensive measurements on another TGS system would benefit this characterization, and this will be discussed further in the paper.

Matrix Uncertainty Component

In order to estimate the uncertainty from matrix effects and the attenuation correction within the image reconstruction, the relative difference of the TGS response across a subset of the point source measurements using the full analysis (Tables 3-5) was compared to an analysis with uniform layer attenuation coefficients (Table 10). The average relative differences (Table 11) for each ROI energy were calculated using Equation 3 as the Matrix Error Component:

$$\sigma_{Matrix} = 1 - \left(\frac{\sum \frac{R_{full}}{R_{uniform}}}{N} \right) \quad (3)$$

where R_{full} is the TGS response number using the full analysis, $R_{uniform}$ is the TGS response number for the same assay using a constant, uniform attenuation factor, and N is the number of assays used.

Table 10 10x10 TGS 120L Uniform Transmission Image Responses

Assay Number	Matrix	276 keV	303 keV	356 keV	384 keV	662 keV	1173 keV	1333 keV
2	FM	0.305	0.711	2.136	0.323	N/A	N/A	N/A
3	FM	0.300	0.705	2.109	0.302	0.407	0.359	0.357
7	SB	0.302	0.698	2.193	0.294	0.400	0.348	0.353
8	SB	0.313	0.737	2.198	0.304	0.408	0.349	0.355
15	MDF	0.254	0.593	1.966	0.265	0.458	N/A	N/A
16	MDF	0.220	0.537	1.778	0.235	N/A	N/A	N/A
17	MDF	0.239	0.555	1.958	0.235	N/A	N/A	N/A
18	MDF	0.235	0.576	1.844	0.256	N/A	N/A	N/A
19	MDF	0.270	0.686	2.079	0.293	N/A	0.360	0.353
20	MDF	N/A	N/A	N/A	N/A	0.394	0.358	0.318
21	MDF	0.297	0.678	2.243	0.308	0.466	0.233	0.242
22	MDF	0.275	0.680	2.240	0.301	0.387	0.313	0.318

Table 11 10x10 TGS 120L Ratio of the Full Response and the Uniform Matrix Response

Assay Number	Matrix	276 keV	303 keV	356 keV	384 keV	662 keV	1173 keV	1333 keV
2	FM	1.007	1.003	1.001	1.009	N/A	N/A	N/A
3	FM	0.997	0.996	0.994	0.997	0.983	1.000	1.000
7	SB	1.027	1.031	1.028	1.024	1.018	1.009	1.011
8	SB	1.036	1.041	1.041	1.034	1.041	1.015	1.014
15	MDF	1.072	1.098	1.116	1.082	1.004	N/A	N/A
16	MDF	1.019	1.008	1.013	1.013	N/A	N/A	N/A
17	MDF	1.044	1.049	1.065	1.059	N/A	N/A	N/A
18	MDF	1.044	1.075	1.063	1.041	N/A	N/A	N/A
19	MDF	1.024	1.016	1.016	1.010	N/A	1.029	1.028
20	MDF	N/A	N/A	N/A	N/A	1.102	1.031	1.017
21	MDF	1.076	1.080	1.070	1.091	1.035	1.069	1.064
22	MDF	1.038	1.056	1.063	1.060	1.040	1.076	1.067
Sum of Ratios		11.382	11.452	11.470	11.419	7.224	7.228	7.203
Average		1.035	1.041	1.043	1.038	1.032	1.033	1.029
Matrix Error		3.5%	4.1%	4.3%	3.8%	3.2%	3.3%	2.9%

Method Uncertainty Component

The method uncertainty component aims to quantify the error introduced when point sources are located at voxel boundaries. Calculation for the method component is based on the same formalism in [6] where three point sources are assumed to be in a given layer and the image reconstructed location of a source is offset by a single voxel width. The following equations used represent the attenuation through a single voxel (f_{voxel}) and the associated uncertainty (σ_{method}):

$$f_{voxel} = e^{-\mu x} \tag{4}$$

$$\sigma_{method} = \frac{\frac{1}{f_{voxel}} - 1}{6 * \sqrt{3}} \tag{5}$$

The value of μ was calculated based on the mass attenuation of cellulose ($C_6H_{10}O_5$) at each matrix density and at each ROI energy. The voxel width, x, in Equation 4 is 4.9 cm for the 120L drum with a 10x10 voxel. Table 12 displays the method uncertainty component as a function of the gamma energy and matrix density.

Table 12 10x10 TGS 120L Method Error Component

Energy (keV)	0.03 g/cc	0.39 g/cc	0.68 g/cc
276	0.2%	2.4%	4.5%
303	0.2%	2.3%	4.4%
356	0.2%	2.1%	4.0%
383	0.1%	2.1%	3.9%
662	0.1%	1.6%	3.0%
1173	0.1%	1.2%	2.2%

TOTAL MEASUREMENT UNCERTAINTY

Based on the components presented in the previous sections, using the available data, the one-sigma (1σ) TMU is calculated as the quadrature sum of the main components shown in Equation 6 below as a function of energy and density. The source location error is shown with both the extreme source locations as well as excluding those particular results in Tables 13 through 15.

$$\sigma_{TMU} = \sqrt{\sigma^2_{calibration} + \sigma^2_{random} + \sigma^2_{source\ location} + \sigma^2_{matrix} + \sigma^2_{method}} \quad (6)$$

The calibration and random components are calculated from the factory calibration effort [5] and based on measurements and analysis outside of this study.

Table 13 TMU Estimate by Energy for the Foam Drum (0.03 g/cc)

Energy (keV)	Calib.	Random	Method	Matrix	Loc.	Loc. with Ends	TMU	TMU With Ends
300-400	9.1%	2.9%	0.3%	4.3%	8.8%	8.8%	14%	14%
662	2.3%	2.3%	0.1%	3.2%	2.1%	4.4%	5%	6%
1173	1.6%	2.2%	0.1%	3.3%	0.1%	8.3%	4%	9%
1333	9.1%	2.4%	0.1%	2.9%	2.2%	8.3%	10%	13%

Table 14 TMU Estimate by Energy for the Softboard Drum (0.39 g/cc)

Energy (keV)	Calib.	Random	Method	Matrix	Loc.	Loc. with Ends	TMU	TMU With Ends
300-400	9.1%	3.3%	3.9%	4.3%	3.4%	3.4%	12%	12%
662	2.3%	2.2%	2.1%	3.2%	1.7%	1.7%	5%	5%
1173	1.6%	2.2%	2.0%	3.3%	1.4%	8.6%	5%	10%
1333	9.1%	2.0%	1.6%	2.9%	0.9%	8.8%	10%	13%

Table 15 TMU Estimate by Energy for the MDF Drum (0.68 g/cc)

Energy (keV)	Calib.	Random	Method	Matrix	Loc.	Loc. with Ends	TMU	TMU With Ends
300-400	9.1%	5.3%	7.9%	4.3%	10.7%	14.8%	17%	20%
662	2.3%	3.4%	3.9%	3.2%	4.6%	5.1%	8%	8%
1173	1.6%	2.9%	3.8%	3.3%	4.7%	7.8%	8%	10%
1333	9.1%	2.9%	3.0%	2.9%	4.1%	6.4%	11%	12%

Investigation of the TGS total measurement uncertainty (TMU) was explored previously in 2003 on the first Canberra TGS for a 208 L drum [6]. For comparison, the TMU values are shown below (Tables 16 and 17) for slightly different matrix densities, but similar trends in terms of energy and matrix type are seen compared to the current 120 L TGS system.

Table 16 200 L TGS System TMU Estimate by Energy for combustibles Drum (0.17 g/cc)

Energy (keV)	Calib.	Random	Method	Matrix	Loc.	TMU
300-400	2.0%	3.0%	1.2%	5.0%	1.3%	6%
662	1.2%	2.0%	0.9%	5.0%	2.1%	6%
1173	1.8%	2.0%	0.7%	5.0%	0.9%	6%
1333	1.8%	2.0%	0.6%	5.0%	1.1%	6%

Table 17 200 L TGS System TMU Estimate by Energy for polyethylene Drum (0.61 g/cc)

Energy (keV)	Calib.	Random	Method	Matrix	Loc.	TMU
300-400	2.0%	7.5%	4.6%	7.0%	5.9%	13%
662	1.2%	5.0%	3.3%	7.0%	3.6%	10%
1173	1.8%	5.0%	2.4%	7.0%	2.3%	9%
1333	1.8%	5.0%	2.2%	7.0%	2.1%	9%

Notable differences from the 200 L TGS system to the current 120 L TGS system are the calibration errors and the source location errors. The calibration methodology for the current system folds in fitting errors in the response curve as well as a larger number of assays to average into the calibration factors than the previous system, where the main error stems from the uncertainty in the calibration source certificates. A wider variation in the positions of the sources was performed in this study including placing sources at the very bottom and very top of the container, so it is not surprising that the estimated error for this component is also larger.

CONCLUSIONS

The performance of a Canberra TGS system designed for 120 L drums has been investigated and evaluated over a wide range of source location within the container. Measurements were performed at several locations using point sources of a number of different nuclide to investigate the response over a wide energy range. A set of matrices containing different matrix densities was also studied and quantified.

The primary reason for the bias is suspected to be due to end effects within the TGS image reconstruction algorithm and possibly attenuation effects from the bottom of the container. Additional measurements were taken with raising the drum, but no significant improvement in the bias resulted. Data similar to this study and a more extensive set will be taken on the next TGS system to further study these effects. An empirical correction factor was developed and implemented within the system's analysis software package to correct this bias for sources found at these extreme vertical layers on this system. Further work is also planned to study the dependence of the collimator opening size, drum size, and volume element definitions on the point-source response.

The impacts of location on the accuracy of attenuation-corrected response to point-like sources for TGS systems were developed further with this study. Comparisons to earlier studies and systems designed for different sized drums were performed and found to be on the same order as previous work. Future work in the both the reconstruction algorithms and end effect corrections are ongoing.

REFERENCES

1. R. Venkataraman, M.F. Villani, S. Croft, P. McClay, R.D. McElroy, S.C. Kane, W..F. Mueller, R.J. Estep, "An Integrated Tomographic Gamma Scanning System for Non Destructive Assay of Radioactive Waste," Nuclear Instruments and Methods A, vol. 579, p. 375-379, 2007.
2. N. Menaa, D. Nakazawa, H. Yang, S. K. Smith, D. L. Petroka, and M. Villani, "An Integrated Waste Assay System Using Tomographic and Segmented Gamma Scanning for Nuclear Power Plant Applications," Paper WM-10375, Proceedings WM'10, March 7-10, 2010 Phoenix, Arizona, USA.
3. J. M. Kirkpatrick, P.J. LeBlanc, D. Nakazawa, D. L. Petroka, S. Kane Smith, R. Venkataraman, and M. Villani, "A Mobile Automated Tomographic Gamma Scanning System," Paper WM-13231, Proceedings WM'13, Feb. 24-28, 2013 Phoenix, Arizona, USA.
4. J. M. Kirkpatrick, D. Nakazawa, S. K. Smith, L. Tondut, P. McClay, D. Petroka, M. Villani, X. Ducoux, and S. Philips, "Recent Advancements in Tomographic Gamma Scanning for Non-Destructive Assay," Paper WM-17321, To be presented at WM2017, March 5-9, 2017, Phoenix, Arizona, USA.

5. J. M. Kirkpatrick, D. Nakazawa, S. K. Smith, L. Tondut, P. McClay, D. Petroka, M. Villani, X. Ducoux, and S. Philips, “High Resolution Scanning Configurations for the Canberra Tomographic Gamma Scanner”, Paper WM-17323, To be presented at WM2017, March 5-9, 2017, Phoenix, Arizona, USA.
6. S. Croft, R. Venkataraman, M. Villani and R.J. Estep, “On the Accuracy of the Tomographic Gamma Scanner for the Assay of Drummed Waste”, Paper WM-4285, Proceedings WM’04, February 29-March 4, 2004 Tucson, Arizona, USA.